© 2019. Published by The Company of Biologists Ltd | Journal of Cell Science (2019) 132, jcs227801. doi:10.1242/jcs.227801

RESEARCH ARTICLE

The juvenility-associated long noncoding RNA *Gm14230* maintains cellular juvenescence

Ayami Tano[1,*], Yosuke Kadota[1,*], Takao Morimune[1,2,*], Faidruz Azura Jam[1], Haruka Yukiue[1], Jean-Pierre Bellier[1], Tatsuyuki Sokoda[2], Yoshihiro Maruo[2], Ikuo Tooyama[1] and Masaki Mori[1,‡]

ABSTRACT

Juvenile animals possess distinct properties that are missing in adults. These properties include capabilities for higher growth, faster wound healing, plasticity and regeneration. However, the molecular mechanisms underlying these juvenile physiological properties are not fully understood. To obtain insight into the distinctiveness of juveniles from adults at the molecular level, we assessed long noncoding RNAs (lncRNAs) that are highly expressed selectively in juvenile cells. The noncoding elements of the transcriptome were investigated in hepatocytes and cardiomyocytes isolated from juvenile and adult mice. Here, we identified 62 juvenility-associated lncRNAs (JAlncs), which are selectively expressed in both hepatocytes and cardiomyocytes from juvenile mice. Among these common (shared) JAlncs, *Gm14230* is evolutionarily conserved and is essential for cellular juvenescence. Loss of *Gm14230* impairs cell growth and causes cellular senescence. *Gm14230* safeguards cellular juvenescence through recruiting the histone methyltransferase Ezh2 to *Tgif2*, thereby repressing the functional role of *Tgif2* in cellular senescence. Thus, we identify *Gm14230* as a juvenility-selective lncRNA required to maintain cellular juvenescence.

KEY WORDS: Long noncoding RNA, lncRNA, Juvenility-associated lncRNAs, JAlncs, Juvenescence, Transcriptome, Bioinformatics

INTRODUCTION

Young animals possess unique traits, such as a higher growth rate, quicker wound healing and faster learning, and also show a higher capability for tissue plasticity and regeneration. These juvenile traits are helpful for the emergence of the mature individual and could provide a therapeutic strategy for intractable diseases. However, the biological and molecular bases behind the regulation of the juvenile traits have been poorly investigated. We previously identified juvenility-associated genes (JAGs) that are highly expressed selectively in juvenile cardiomyocytes and hepatocytes in mice (Jam et al., 2018). Here, we analyzed the noncoding elements of the transcriptome to obtain a comprehensive landscape of the transcriptome regulating cellular juvenescence.

lncRNAs are transcripts of more than 200 nucleotides that do not encode for proteins (Kopp and Mendell, 2018; Mercer et al., 2009; Ponting et al., 2009; Rinn and Chang, 2012; Wilusz et al., 2009). Preceding studies have reported that the genome is pervasively transcribed and contains numerous transcriptional units with unknown function (Bertone et al., 2004; Hangauer et al., 2013; Kapranov et al., 2007a,b; Xu et al., 2009). The current understanding of the expression patterns and functions of the lncRNA molecular group is incomplete, although recent studies have identified lncRNAs in the human transcriptome with accurate 5′ ends (Hon et al., 2017).

During cellular senescence, the lncRNA *MIR31HG* de-represses the transcription of $p16^{INK4A}$ (also known as *CDKN2A*), thus mediating *B-RAF*-induced cellular senescence (Vanderschuren et al., 1997). The *PANDAR* lncRNA interacts with scaffold-attachment-factor A (SAFA, also known as HNRNPU) and polycomb repressive complexes (PRCs), thus suppressing senescence in proliferating cells (Puvvula et al., 2014).

Numerous lncRNAs function as 'scaffolds' for chromatin-modifying complexes (Khalil et al., 2009). The *Xist* lncRNA functions by recruiting polycomb repressive complex 2 (PRC2) to one of the X chromosomes in cells from females, repressing its transcription and dose-compensating X chromosome gene expression (Brockdorff et al., 1991; Zhao et al., 2008). *Hotair*, which is encoded by the *HoxC* locus, represses *HoxD* genes by recruiting PRC2 to the *HoxD* locus (Rinn et al., 2007). Braveheart (*Bvht*) interacts with Suz12, a PRC2 component, during cardiomyocyte differentiation, thereby regulating gene expression (Klattenhoff et al., 2013). *PANDAR* recruits PRC1 and PRC2 to specific gene loci, including *CDKN1A* (Puvvula et al., 2014). *Fendrr* binds the PRC2 and TrxG/MLL complexes, thereby regulating gene function during heart development (Grote et al., 2013). *Airn* recruits the histone methyltransferase G9a (also known as Ehmt2) to a target gene locus for gene silencing (Braidotti et al., 2004; Nagano et al., 2008).

Although the molecular machinery by which lncRNAs perform their functions have been investigated as described above, knowledge regarding the age-dependent functions of lncRNAs, particularly their functions during the juvenile phase, is limited. Here, we established a lncRNA analysis bioinformatics pipeline and identified juvenile-selective lncRNAs. These lncRNAs, which we call juvenility-associated lncRNAs (JAlncs), constitute a transcriptional network responsible for the juvenile properties of a cell. Furthermore, *Gm14230* (ENSMUSG00000087179), which is an evolutionarily conserved JAlnc, maintains the juvenile properties of cells, and the loss of *Gm14230* promotes cellular senescence. Thus, our lncRNA analysis identified the noncoding elements in the transcriptome network controlling the juvenile properties of cells.

RESULTS

Identification of juvenility-associated lncRNAs

To identify lncRNAs that are highly expressed selectively in juvenile cells, we established a pipeline to analyze the nucleotide sequence of the noncoding transcripts extracted from mouse

[1]Molecular Neuroscience Research Center (MNRC), Shiga University of Medical Science, Seta Tsukinowa-cho, Otsu, Shiga 520-2192, Japan. [2]Department of Pediatrics, Shiga University of Medical Science, Seta Tsukinowa-cho, Otsu, Shiga 520-2192, Japan.
*These authors contributed equally to this work

‡Author for correspondence (morim@belle.shiga-med.ac.jp)

M.M., 0000-0001-7632-3875

Received 13 November 2018; Accepted 5 March 2019

Journal of Cell Science (2019) 132, jcs227801. doi:10.1242/jcs.227801

hepatocytes and cardiomyocytes at different times during postnatal development (Fig. 1A). The original dataset was generated in a previous work of ours (Jam et al., 2018) and deposited in the DNA Data Bank of Japan (DDBJ) under the accession number DRA007101 (https://ddbj.nig.ac.jp/DRASearch/submission?acc=DRA007101). Thus, we analyzed the lncRNAs in the transcriptome of hepatocytes and cardiomyocytes isolated from juvenile [postnatal day (P)1 and P7] and adult (P56) mice (n=3, Fig. 1A). P1 and P7 correspond to an early and late neonatal phase in mice, respectively. Two points (P1 and P7) rather than one were included to capture consistent alterations in comparison to the adult phase (P56). The Ensembl database (version 91.38) (Zerbino et al., 2018) covers 5034 lncRNAs in the mouse transcriptome. We defined the juvenility-associated lncRNAs (JAlncs) as lncRNAs that were more highly expressed in juvenile (both at P1 and P7) cells than adult (P56) cells by more than 2-fold. Consequently, we identified 327 JAlncs in the hepatocytes (hepato-JAlncs) and 262 JAlncs in the cardiomyocytes (cardio-JAlncs) (Fig. 1A).

Then, we analyzed the components of the hepato- and cardio-JAlncs. The hepato-JAlncs included functionally well annotated lncRNAs, such as *H19*, *Lockd* and *Snhg5* (Fig. 1B). The adult (P56)-expressed lncRNAs included *Lncbate1* (Fig. 1B). The cardio-JAlncs also included functionally annotated lncRNAs, such as *H19*, *Xist*, *Jpx* and *Crnde* (Fig. 1C). The results of the previous RNA-seq analysis (Jam et al., 2018) were validated by quantitative PCR (qPCR) (Fig. 1D). Thus, we identified JAlncs in juvenile hepatocytes and cardiomyocytes in mice.

Identification of common JAlncs and *Gm14230*

To identify lncRNAs that play an essential role in the juvenile physiology, we focused on the JAlncs common (shared) between the hepato- and the cardio-JAlncs. While numerous lncRNAs are expressed in a tissue-specific manner (Cabili et al., 2015; Washietl et al., 2014), others including *MALAT1* are broadly expressed (Ji et al., 2003; Nakagawa et al., 2012), indicating their important function for all types of cells. A total of 62 lncRNAs were identified as the common JAlncs by retrieving the overlapping lncRNAs between the hepato- and cardio-JAlncs (Fig. 2A,B). The expression data of the 62 common JAlncs are shown in Table S1. The common JAlncs included *H19*, *Lockd*, *Snhg5*, *Crnde*, *Meg3* and *Rian* (Fig. 2C).

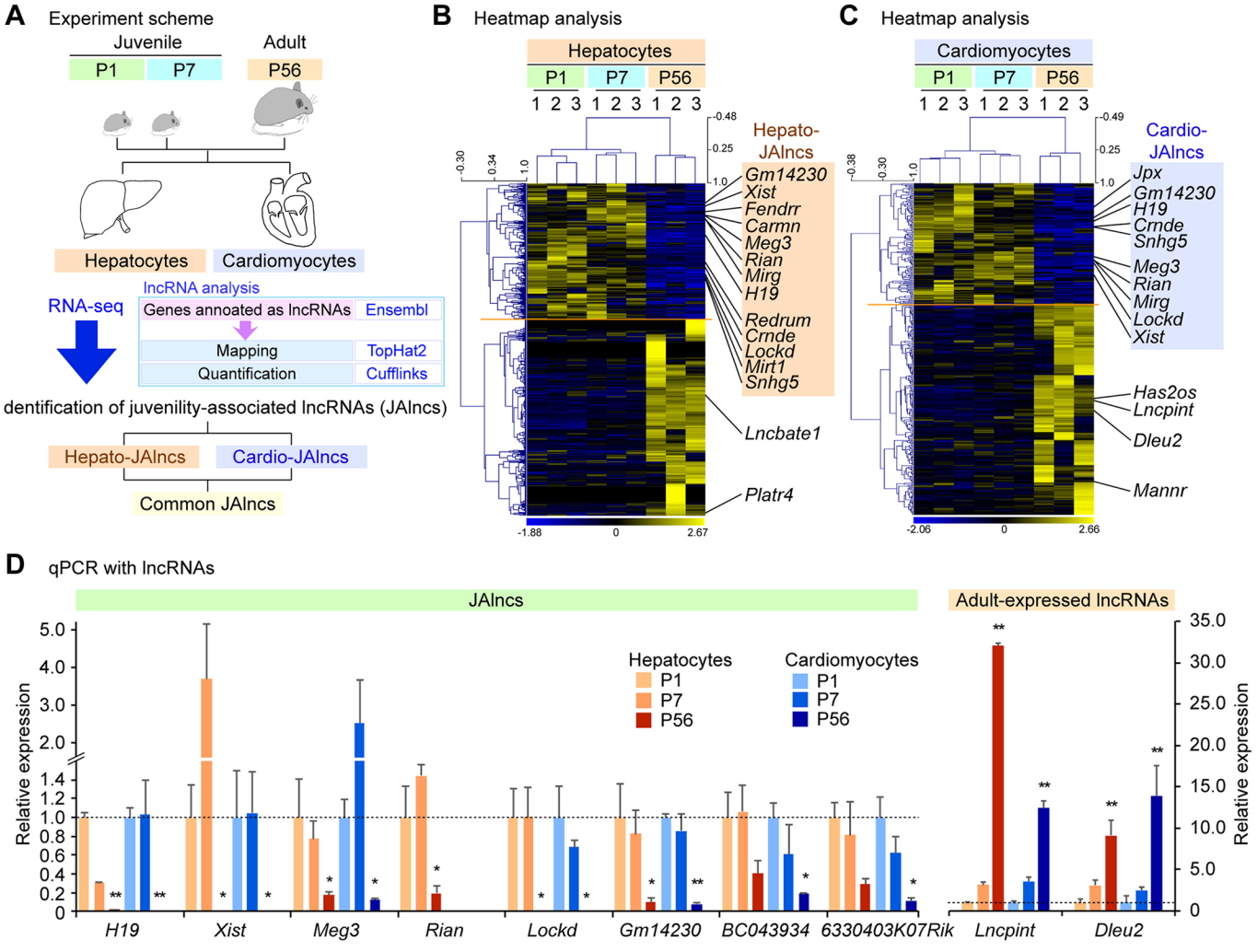

Fig. 1. Identification of JAlncs in mouse hepatocytes and cardiomyocytes. (A) Schematic describing the identification of the juvenility-associated lncRNAs (JAlncs). Detailed procedures for the lncRNA bioinformatics analysis are described in the Materials and Methods. Hepato-, hepatocyte; Cardio-, cardiomyocyte; P, postnatal day. (B) Heatmap analysis of the transcriptome in mouse hepatocytes at different ages. (C) Heatmap analysis of the transcriptome in mouse cardiomyocytes at different ages. (D) qPCR analysis of common JAlncs and adult-expressed lncRNAs in the hepatocytes and cardiomyocytes. Data were normalized to *Polr2a*. **P*<0.05, ***P*<0.01. Data are represented as the mean±s.d. from three biological replicates.

Journal of Cell Science (2019) 132, jcs227801. doi:10.1242/jcs.227801

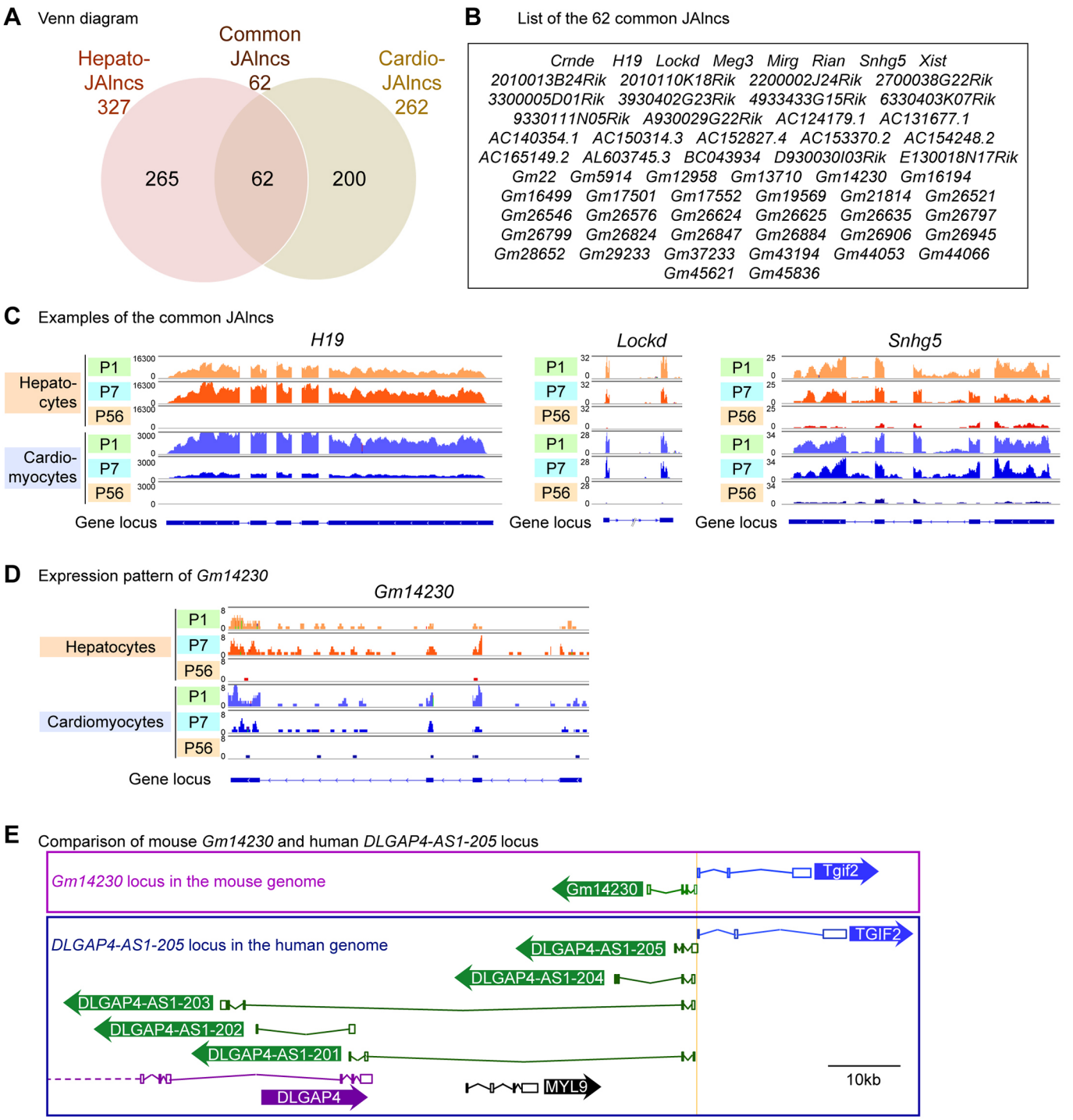

Fig. 2. *Gm14230* is an evolutionarily conserved common JAlnc. (A) Venn diagram showing the common JAlncs as overlapping genes between the hepato- and cardio-JAlncs. (B) List of 62 common JAlncs. (C) Integrative Genomics Viewer (IGV) presentation of the expression of the representative shared JAlncs *H19*, *Lockd* and *Snhg5*. The height indicates fragments per kilobase of transcript per million mapped reads (FPKM). (D) IGV presentation of the expression of *Gm14230*. (E) Genomic view showing the exons and introns of the mouse *Gm14230-Tgif2* locus and human *DLGAP4-AS1-205-TGIF2* locus.

The common JAlncs also included numerous lncRNAs with unknown functions. With the aim to discover novel lncRNAs and their functions to broaden our understanding of the molecular machinery of the juvenile transcriptome, we focused on the JAlncs with an unknown function. Based on the hypothesis that functionally important lncRNAs are evolutionarily better conserved, we investigated interspecies conservation of the common JAlncs. A BLAST search identified a homologous lncRNA in human for 17 common JAlncs (Table S2), of which nine were novel. We compared a secondary structure of the conserved JAlncs, because a lncRNA sequence is not generally well conserved. The predicted secondary structures of lncRNAs were compared using RNAforester (Höchsmann et al., 2003, 2004). We identified *Gm14230* (Fig. 2D) as having the highest similarity to a human homolog in the secondary structure among the conserved JAlncs (Table S2). An open reading frame analysis with ORFfinder

Journal of Cell Science (2019) 132, jcs227801. doi:10.1242/jcs.227801

(https://www.ncbi.nlm.nih.gov/orffinder/) showed *Gm14230* had a potential to code a peptide consisting of up to 70 amino acids. The gene encoding *Gm14230* is adjacent to the *Tgif2* gene in the mouse genome (Fig. 2E). In the human genome, the *DLGAP4-AS1* lncRNA gene is adjacent to *TGIF2* (Fig. 2E). The sequence of *Gm14230* is similar to that of the *DLGAP4-AS1* variant *DLGAP4-AS1-205* (62.4% match, Fig. S1A). *DLGAP4-AS1-205* is not considered an antisense transcript of *DLGAP4* because they do not overlap, and *DLGAP4-AS1-205* has exon–intron patterns that are distinct from those of other *DLGAP4-AS1* variants (201, 202, 203 and 204) (Fig. 2E). Similar to *Gm14230*, *DLGAP4-AS1-205* has not been functionally annotated.

The proximity of *Gm14230* to *Tgif2* suggests that these two genes are coordinately regulated. The coordinated regulation of a lncRNA and a protein-coding gene is a frequently observed phenomenon (Hon et al., 2017; Sigova et al., 2013). An analysis using the ChIP-Atlas (http://chip-atlas.org), which is a comprehensive database of previous ChIP-seq findings, revealed dense histone modifications associated with the active promoter (H3K4me3 and H3K9ac) upstream of *Gm14230* in the first intron of *Tgif2* in the mouse liver, heart and embryonic fibroblasts (Fig. S1B). Therefore, *Gm14230* is likely regulated by a bidirectional promoter present in the first intron of *Tgif2* that regulates both *Gm14230* and *Tgif2*. Thus, we identified the common JAlncs and selected *Gm14230* for further functional analysis.

Gm14230 undergoes A-to-I RNA editing

Based on the hypothesis that a variant of *Gm14230* might exist, we cloned the *Gm14230* cDNA from NIH3T3 cells. Sequence analysis in *Gm14230* revealed an adenosine (A) to guanosine (G) mutation in half (5 of 10) of the clones (Fig. S2A). This nucleotide alteration was also observed in the mouse neonatal hepatocytes (Fig. S2B). The recurrent substitution implied that *Gm14230* is a substrate for adenosine to inosine (A-to-I) RNA editing (Gott and Emeson, 2000; Kawahara et al., 2007; Nishikura, 2010; Sommer et al., 1991; Zheng et al., 2016). Because inosine (I) base-pairs with cytosine (C), I is recognized as G by sequencing after cDNA synthesis. To investigate whether the nucleotide change is due to A-to-I editing, we performed cyanoethylation on the extracted RNA (Suzuki et al., 2015). Acrylonitrile treatment induces the cyanoethylation of inosine bases (ce^1I), and ce^1I does not base-pair with C and prevents cDNA synthesis. The acrylonitrile treatment of the RNA extracted from the NIH3T3 cells resulted in a decrease of the G peak (Fig. S2C), corroborating the idea that *Gm14230* undergoes A-to-I editing. We further hypothesized the RNA editing of *Gm14230* might have a functional relevance. We investigated an age-dependency of the RNA editing of *Gm14230* and found the A-to-I editing was more frequent in cardiomyocytes derived from older mice (Fig. S2D). These results suggest that the function of *Gm14230* is modified through RNA editing in the age-dependent manner.

Subcellular localization of *Gm14230*

The subcellular localization of lncRNAs has been systematically investigated in human cells (Mas-Ponte et al., 2017) but not in mouse cells. To investigate the subcellular localization of the *Gm14230* lncRNA, we performed RNA-FISH and found *Gm14230* localized both in the cytoplasm and nucleus (Fig. S3A). For a more quantitative analysis, we performed subcellular fractionation followed by qPCR analysis. This analysis showed that approximately two thirds of *Gm14230* localized in the cytoplasm, and one third in the nucleus (Fig. S3B). Serving as control, primary (pri)-microRNAs, which are precursors of microRNAs serving as substrates for the so-called microprocessor complex in the nucleus (Gregory et al., 2004), were detected almost exclusively in the nuclear fraction, and *Actb* mRNA was detected mainly in the cytoplasmic fraction (Fig. S3B). We also tested the hypothesis that different cell densities could affect localization, but the *Gm14230* subcellular localization was not significantly altered by the cell densities (Fig. S3B). Then, we examined whether cytoplasmic *Gm14230* returns to the nucleus after cytoplasmic distribution following transcription. RNAi operating in the cytoplasm (Zeng and Cullen, 2002), if *Gm14230* cannot translocate from the cytoplasm back to the nucleus, therefore RNAi cannot decrease the *Gm14230* levels in the nucleus. The siRNA-mediated knockdown of *Gm14230* leads to a decrease in *Gm14230* in the nucleus, implying that the *Gm14230* lncRNA shuttles between the cytoplasm and nucleus (Fig. S3C).

We further evaluated whether the fibroblast aging affected the subcellular localization of *Gm14230*. We induced cellular senescence by using the genotoxic agent zeocin (Fig. S3D; Mao et al., 2016; Robles and Adami, 1998). *Gm14230* expression was repressed in the senescent cells, and the decrease was more significant in the cytoplasm than the nucleus, suggesting a cytoplasmic machinery that downregulates *Gm14230* (Fig. S3E,F). These findings suggest that the amount of nuclear *Gm14230* is regulated under the control of equilibrium that is affected by cellular aging.

Gm14230 loss impairs growth and induces senescence

To determine the biological relevance of *Gm14230*, we repressed *Gm14230* by using siRNA in mouse NIH3T3 cells (Fig. 3A). In this experiment, we utilized three different siRNAs to distinguish any possible off-target effects. The *Gm14230* knockdown using each of the three siRNAs significantly suppressed cell growth (Fig. 3B,C). The knockdown of a different JAlnc, *AC153370.2*, did not affect cell growth suggesting that the effect on *Gm14230* is specific (Fig. S4A–C). *Gm14230* knockdown decreased the number of Ki67-positive cells, suggesting that it induced cell cycle exit (Fig. S4D). In addition, *Gm14230* knockdown did not increase the number of cells positive for active caspase 3 (Fig. S4E) or cleaved PARP (Fig. S4F), indicating that the growth suppression was not accompanied by apoptosis. We also noticed that the *Gm14230* knockdown induced changes in the cell shape, such as a flattened and extended cytoplasm, reminiscent of senescent cells (Serrano et al., 1997). β-galactosidase staining, which is associated with senescence (Serrano et al., 1997), showed significantly increased positivity in cells transfected with siRNA against *Gm14230* (Fig. 3D,E). Similar findings were observed with *DLGAP4-AS1-205* in human ONS-76 cells (Fig. S4G–I). Furthermore, *Gm14230* knockdown induced growth impairment (Fig. S4J–L) and cellular senescence (Fig. S4M,N) in Hepa1-6 cells, suggesting that *Gm14230* has a functional relevance of in the hepatocytes in which *Gm14230* was identified. Moreover, *Gm14230* knockdown led to the induction of the senescence-associated proteins P16 (Alcorta et al., 1996), P27 (also known as CDKN1B) (Collado et al., 2000) and the marker γH2Ax (Fagagna et al., 2003) in NIH3T3 cells (Fig. 3F). *Gm14230* knockdown also suppressed the protein expression of Srsf7, which is a juvenility-associated gene (JAG) that is highly expressed in juvenile cells (Jam et al., 2018) (Fig. 3F). Taken together, these observations indicate that the loss of *Gm14230* leads to cellular growth impairment and cell senescence.

Gm14230 represses *Tgif2* transcription through Ezh2 recruitment

Subsequently, we sought to determine the mechanism by which *Gm14230* regulates cell growth. *Gm14230*-adjacent *Tgif2* belongs

Journal of Cell Science (2019) 132, jcs227801. doi:10.1242/jcs.227801

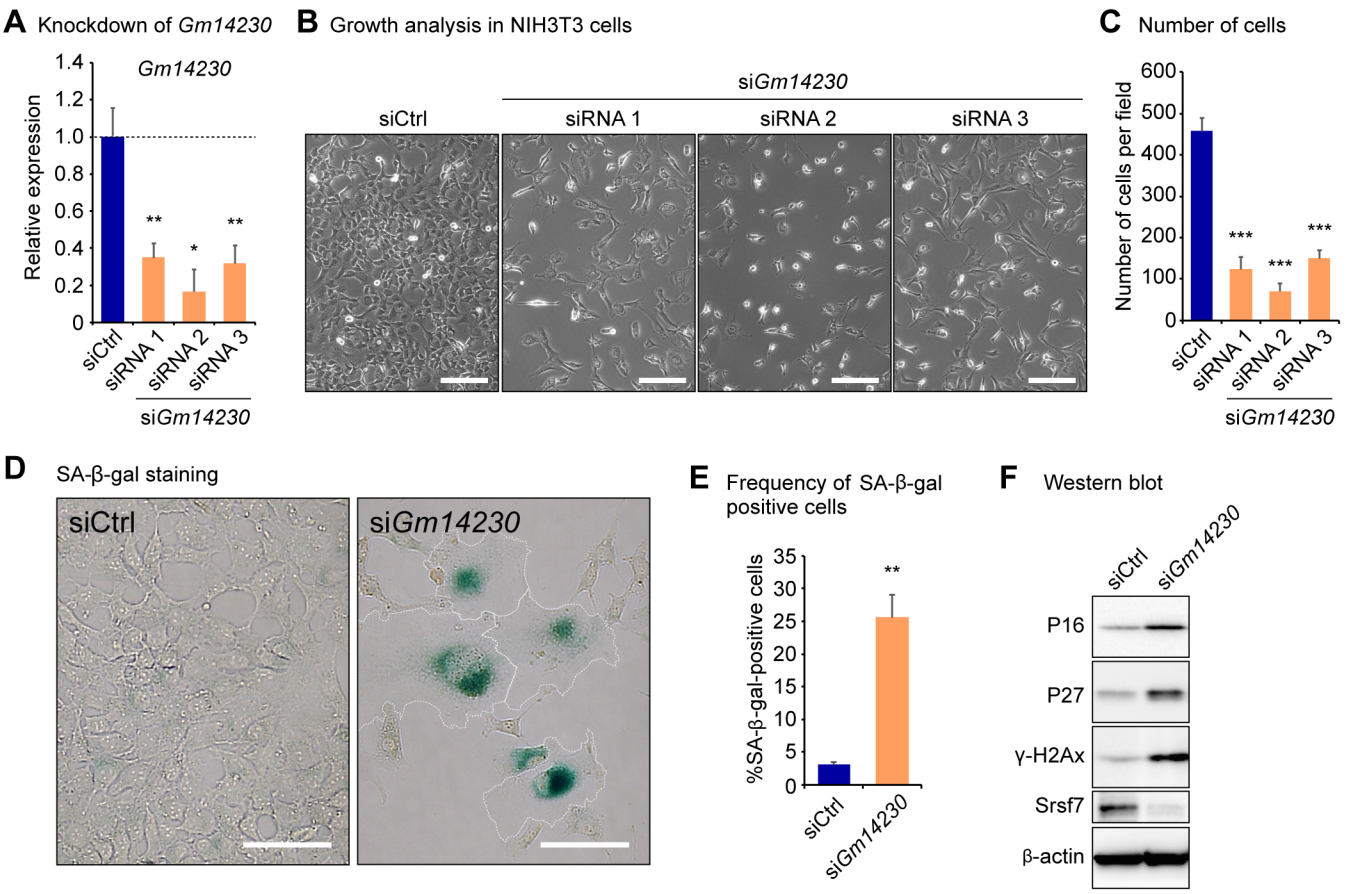

Fig. 3. *Gm14230* loss impairs growth and induces senescence. (A) qPCR analysis of *Gm14230* in NIH3T3 cells transfected with control siRNA (siCtrl) or siRNA against *Gm14230* (si*Gm14230*; siRNA 1, siRNA 2, siRNA 3). Data were normalized to expression of *Tubb5*. Data are from three independent experiments, and error bars indicate s.d. **P*<0.05, ***P*<0.01. (B) Appearance of NIH3T3 cells 72 h after transfection with control siRNA or siRNA against *Gm14230*. Scale bars: 200 µm. (C) Number of cells per field 72 h after transfection with control siRNA or siRNA against *Gm14230*. ****P*<0.001. Data are the mean±s.d. from three independent experiments. (D) Staining of SA-β-gal activity in cells after transfection with control siRNA or siRNA against *Gm14230*. White dotted lines outline the edge of the cells in panel 'si*Gm14230*'. Scale bars: 100 µm. (E) Frequency of cells positive for the SA-β-gal staining per field. *n*=301 and 105 cells; data are the mean±s.d. from three independent experiments. ***P*<0.01. (F) Western blot analysis of senescence-associated proteins (P16, P27 and γH2Ax) and the juvenility-associated protein Srsf7. β-actin was used as a loading control.

to a family of genes encoding TALE-homeodomain proteins, including *Tgif1*, *Tgif2* and *Tgif2lx1*. Tgif2 functions as a transcriptional repressor and suppresses transcription initiated by TGF-β (Melhuish et al., 2001). *Gm14230* knockdown enhanced *Tgif2* mRNA expression in the NIH3T3 cells, suggesting that *Gm14230* functions as a negative regulator of *Tgif2* expression (Fig. 4A). To assess the regulation of *Tgif2* by *Gm14230* further, we examined an expression of *Evi5l*, a transcriptional target of Tgif2 (Anderson et al., 2017). *Gm14230* knockdown significantly downregulated *Evi5l*, while the effect was abolished by simultaneous knockdown of *Gm14230* and *Tgif2* (Fig. 4A). This observation indicates that *Gm14230* regulates *Evi5l* through *Tgif2*.

Next, we aimed to identify the partner required for *Gm14230* to repress *Tgif2*. lncRNAs, such as *Xist* (Brockdorff et al., 1991; Zhao et al., 2008), *Hotair* (Rinn et al., 2007), *Bvht* (Klattenhoff et al., 2013), *Pandar* (Puvvula et al., 2014), *Fendrr* (Grote et al., 2013) and *Airn* (Braidotti et al., 2004; Nagano et al., 2008), interact with the PRC complex and induce gene silencing. Thus, the interactions between *Gm14230* and Ezh2, which is a component of the PRC2 complex, were assessed. RNA immunoprecipitation and subsequent qPCR (RIP-qPCR) analyses revealed that *Gm14230* bound the Ezh2 protein in NIH3T3 cells (Fig. 4B). Furthermore, the re-analysis of the RNA immunoprecipitation-sequencing (RIP-seq) that comprehensively identified the Ezh2-bound transcriptome (Zhao et al., 2010), revealed interactions between *Gm14230* and Ezh2 in mouse embryonic stem cells (Fig. S5A).

To directly assess the role of *Gm14230* in Ezh2 recruitment to *Tgif2* locus, we performed chromatin immunoprecipitation (ChIP) analysis for Ezh2 protein in normal and *Gm14230*-knockdown NIH3T3 cells. Among the evolutionarily conserved sequence near the *Tgif2* transcription start site (Fig. 4C), two loci in the *Tgif2* first intron showed significant enrichment when immunoprecipitated by Ezh2 (Fig. 4D). siRNA-mediated depletion of *Gm14230* abrogated the occupation of *Tgif2* loci by Ezh2, indicating the pivotal role of *Gm14230* for the recruitment of Ezh2 at these loci (Fig. 4D). *H1foo*, which is expressed in an oocyte-specific manner (Teranishi et al., 2004), showed Ezh2 occupation regardless of *Gm14230* expression (Fig. 4D). Thus, *Gm14230* recruits Ezh2 to the *Tgif2* regulatory elements, thereby repressing *Tgif2* transcription (Fig. 4E).

Gm14230 safeguards cellular juvenescence by repressing *Tgif2*

We then investigated the biological relevance of *Tgif2* expression on cell growth. Compared to the *EGFP* control, overexpression of *Tgif2* significantly suppressed the growth of NIH3T3 cells (Fig. 5A,B). The growth suppression was

Journal of Cell Science (2019) 132, jcs227801. doi:10.1242/jcs.227801

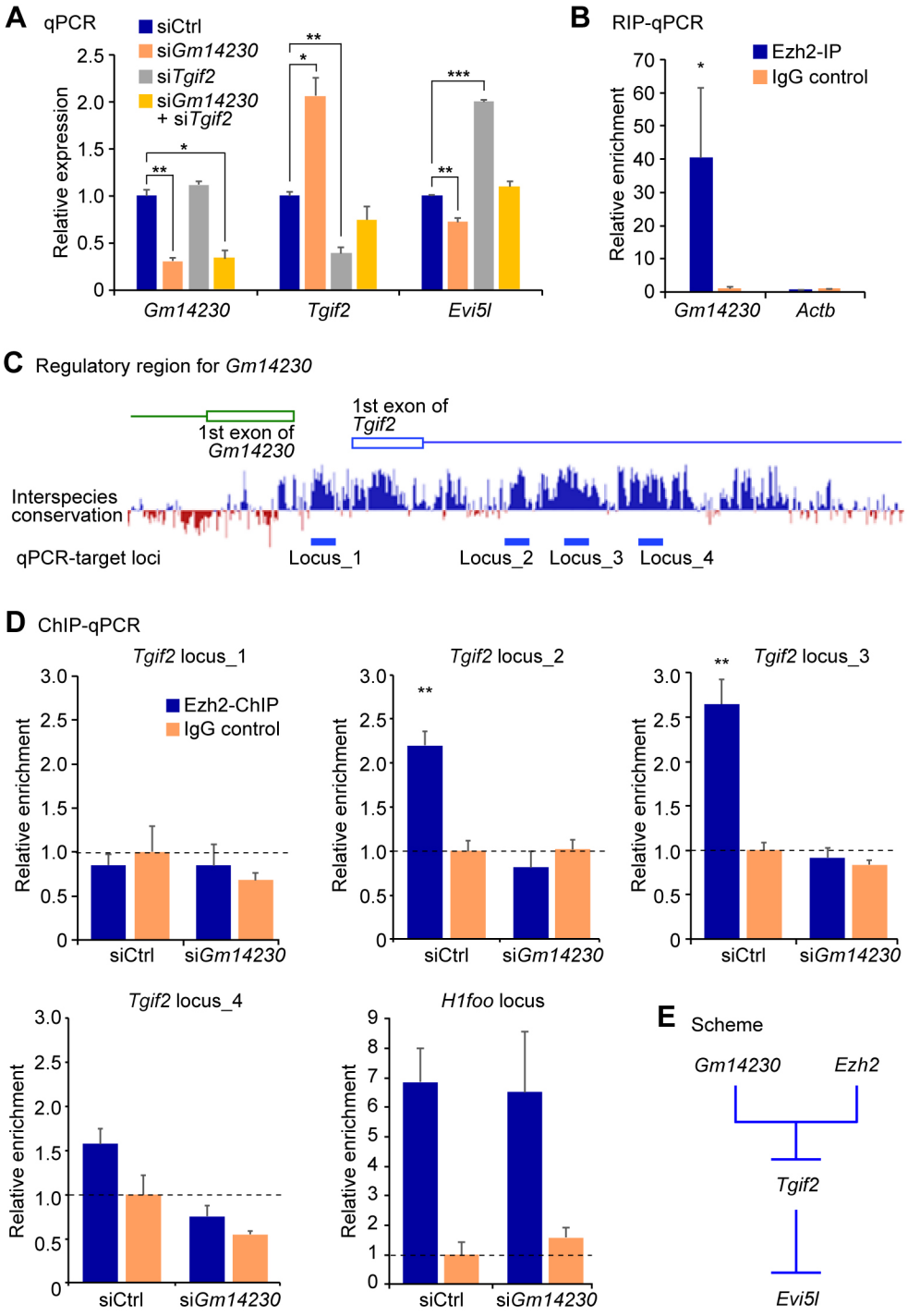

Fig. 4. *Gm14230* represses *Tgif2* transcription through Ezh2 recruitment. (A) qPCR analysis of *Gm14230*, *Tgif2* and *Evi5l* in NIH3T3 cells transfected with the indicated siRNAs (siCtrl, control siRNA; si*Gm14230*, siRNA against *Gm14230*; si*Tgif2*, siRNA against *Tgif2*). RNA was extracted 48 h after transfection. Data were normalized to *Tubb5*. Data are from three independent experiments, and error bars indicate s.d. **P*<0.05, ***P*<0.01, ****P*<0.001. (B) RIP-qPCR analysis using an Ezh2 antibody or control IgG in NIH3T3 cells. *Gm14230* or control *Actb* RNA was quantified by qPCR after the immunoprecipitation with Ezh2 or control IgG antibody. Relative enrichment in comparison to the IgG were shown. Data are from three independent experiments, and error bars indicate s.d. **P*<0.05. (C) Interspecies conservation near the *Tgif2* transcription start site. The data and the image for the conservation were taken from the UCSC genome browser. The target loci for the chromatin immunoprecipitation (ChIP) is also indicated. The height of the histogram reflects the magnitude of the conservation score. (D) ChIP-qPCR analysis examining the occupancy by Ezh2 at the *Tgif2* loci and the silent histone gene *H1foo*, as a control locus, in NIH3T3 cells. Data were normalized to the value seen with IgG immunoprecipitation performed in the control siRNA-transfected cells. Data are from three independent experiments, and error bars indicate s.d. ***P*<0.01. (E) Schematic describing the cooperative function of *Gm14230* and Ezh2 repressing *Tgif2*.

accompanied by decreased levels of Ki67 (Fig. S5B) but no active caspase 3 (Fig. S5C) or cleaved PARP (Fig. S5D) was detected, excluding the involvement of apoptosis. Moreover, the *Tgif2*-transfected cells exhibited an extended cytoplasm and positive staining for senescence-associated β-galactosidase (SA-β-gal) activity, indicating that enhanced *Tgif2* expression leads to cell senescence (Fig. 5C,D). The *Tgif2*-transfected cells expressed the senescence-associated proteins P16, P27 and γH2Ax (Fig. 5E).

To investigate the role of *Gm14230–Tgif2* axis in senescence induction, we performed simultaneous knockdown of *Gm14230* and *Tgif2*. A significant rescue of the cell growth impairment that was seen with *Gm14230* knockdown alone was observed (Fig. 5F,G), thus confirming the function of *Tgif2* in combination with *Gm14230*. In addition, the simultaneous knockdown decreased the positive staining for SA-β-gal activity induced by *Gm14230* knockdown (Fig. 5H,I), supporting the notion that *Gm14230* regulates the cellular juvenescence by repressing *Tgif2*. Knockdown of *Evi5l*, a downstream target of *Gm14230-Tgif2* axis, neither impaired cell growth (Fig. S5E–G) nor induced cell senescence (Fig. S5H), suggesting that *Evi5l* is not used by *Gm14230–Tgif2* axis to regulate the cell senescence. Collectively, *Gm14230* regulates cell growth and titrates *Tgif2* expression to avoid undergoing cell senescence (Fig. 6). Taken together, the analysis of the observations from this study has revealed the essential roles of

Journal of Cell Science (2019) 132, jcs227801. doi:10.1242/jcs.227801

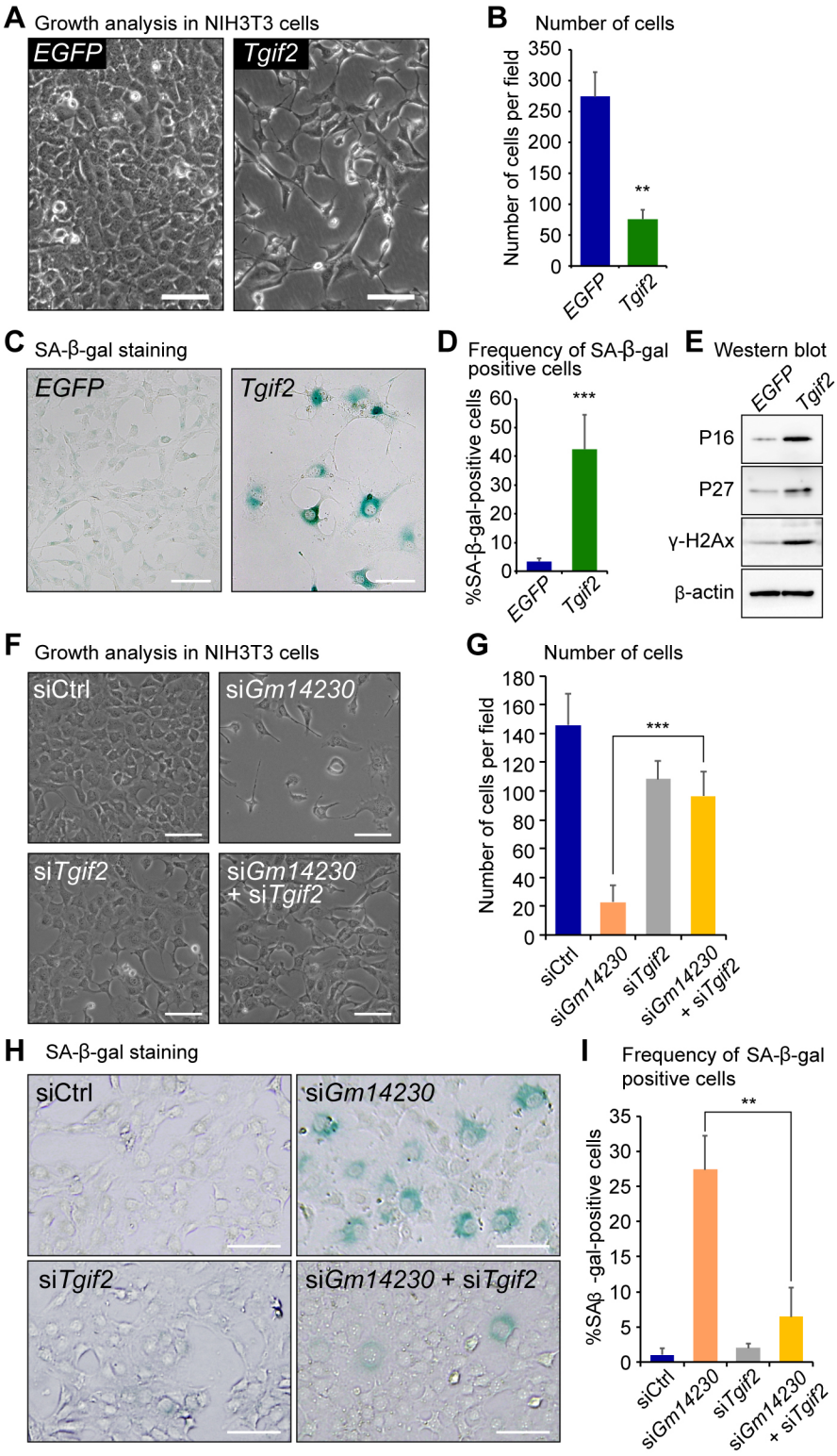

Fig. 5. *Gm14230* maintains cellular juvenescence via *Tgif2*. (A) Appearance of NIH3T3 cells 72 h after transfection with control *EGFP* or *Tgif2*. Scale bar: 100 µm. (B) Number of cells per field 72 h after the transfection with control *EGFP* or *Tgif2*. Data are the mean±s.d. from three independent experiments. $^{**}P<0.01$. (C) Staining of SA-β-gal activity in cells after transfection with control *EGFP* or *Tgif2*. Scale bars: 100 µm. (D) Frequency of SA-β-gal-positive cells per field. $^{***}P<0.001$. n=449 and 104 cells. Data are the mean±s.d. from three independent experiments. (E) Western blot analysis of senescence-associated proteins (P16, P27 and γH2Ax). β-actin was used as a loading control. (F) Appearance of NIH3T3 cells 72 h after transfection of the indicated siRNAs (siCtrl, control siRNA; si*Gm14230*, siRNA against *Gm14230*; si*Tgif2*, siRNA against *Tgif2*). Scale bars: 200 µm. (G) Number of cells per field 72 h after transfection of the siRNAs. Data are the mean±s.d. from three independent experiments. $^{***}P<0.001$. (H) Staining of SA-β-galactosidase activity in the NIH3T3 cells after transfection of the siRNAs. Scale bars: 100 µm. (I) Frequency of SA-β-gal-positive cells per field. Data are the mean±s.d from three independent experiments. $^{**}P<0.01$; n=284, 124, 247 and 197 cells.

JAlncs, which are lncRNAs that are highly expressed selectively in juvenile cells. Moreover, *Gm14230* is an indispensable factor that regulates cell growth and cellular juvenescence.

DISCUSSION

In this study, we performed a comprehensive lncRNA analysis in differentially aged cardiomyocytes and hepatocytes to identify lncRNAs that are highly expressed selectively in juvenile cells. Among the juvenility-associated lncRNAs (JAlncs), we identified *Gm14230* as an essential factor for the maintenance of cellular juvenescence. The cellular juvenile properties, including the higher proliferation, differentiation and maturation abilities, have a tendency to be lost during cell senescence. Molecules involved in cellular juvenescence might increase the ability of cells to proliferate and regenerate, and, hence, counteract cellular senescence. As demonstrated by the depletion of the JAlnc *Gm14230* causing

Journal of Cell Science (2019) 132, jcs227801. doi:10.1242/jcs.227801

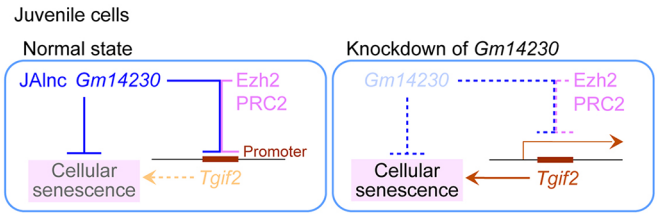

Fig. 6. Regulation of cellular juvenescence by *Gm14230*. Schematic describing the functions of *Gm14230* that regulate cell growth and inhibit cell senescence via the transcriptional repression of *Tgif2*.

premature senescence in the various cell types, a role of the JAlncs is to maintain the juvenile state to counteract senescence.

Since the discovery that the genome is pervasively transcribed, numerous lncRNAs have been functionally investigated. Among JAlncs, *Lockd* is an enhancer RNA transcribed from an enhancer of the *Cdkn1A* gene (Paralkar et al., 2016), *Snhg5* promotes cancer cell proliferation (Damas et al., 2016) and *Crnde* is associated with cancer progression (Ellis et al., 2012). Adult-expressed lncRNAs include *Lncbate1*, which is associated with mitochondrial biogenesis (Alvarez-Dominguez et al., 2015).

lncRNAs have the potential to serve as therapeutic targets; specifically targeting a lncRNA via an oligonucleotide, such as siRNA or antisense oligonucleotide (ASO), is possible and has been clinically applied for the treatment of spinal muscular atrophy (Lim and Hertel, 2001) and Duchenne muscular dystrophy (van Deutekom, 2001). Whenever JAlncs might be associated with intractable human diseases, they might as well become a therapeutic target via an oligonucleotide.

Gm14230 expression is age dependent and is virtually non-existent in adult cells in mouse hepatocytes and cardiomyocytes. As shown by the ChIP-atlas analysis of histone modifications, *Gm14230* transcription can be regulated by the promoter present in the first intron of *Tgif2*. This regulatory element is also likely to regulate the transcription of *Tgif2* because a region with a similar histone modification does not exist around the *Tgif2* transcription start site (TSS). Divergent or bidirectional promoters are frequently observed to regulate lncRNA and protein-coding gene pairs (Hon et al., 2017; Sigova et al., 2013). Elucidating the mechanism by which the divergent promoter of *Gm14230* and *Tgif2* is silenced in an age-dependent manner may reveal the mechanistic machinery involved in the loss of juvenility and initiation of aging.

We found that the subcellular localization of *Gm14230* is maintained at an equilibrium between the nucleus and the cytoplasm (Fig. S3). The perturbation of the equilibrium occurred in the premature senescent cells, resulting in a lower *Gm14230* expression in the cytoplasm, implying that a cytoplasmic machinery downregulates *Gm14230*. One aspect of the cytoplasmic machinery might involve microRNAs. lncRNAs are targets for miRNA-mediated degradation, as in the case of *Hottip* lncRNA, which is targeted by *miR-192* and *204* (Ge et al., 2015). *Gm14230* contains multiple potential target sites for miRNAs (Fig. S6A), and the expression of *Gm14230* is enhanced in *Dicer*-deficient mouse embryonic stem cells (Zheng et al., 2014), *Dicer*-deficient spermatocytes (Modzelewski et al., 2015) and *Ago2*-deficient embryonic stem cells (Ngondo et al., 2018; Fig. S6B). These findings implied the cytoplasmic expression of *Gm14230* might be regulated by microRNAs.

Our analysis also discovered *Gm14230* is a substrate for the A-to-I RNA editing. A biological role for the RNA editing of lncRNAs is not fully understood. An alteration of the sequence is considered to change an affinity for binding with other molecular species such as DNA (Batista and Chang, 2013), RNA (Jalali et al., 2013), protein (Ferrè et al., 2016) and others, thereby influencing the downstream molecular function of a lncRNA. Further elucidation of the effects of RNA editing might reveal an as yet unknown role for the RNA editing of lncRNAs.

The *Gm14230* knockdown led to enhanced *Tgif2*, indicating that the *Gm14230* lncRNA represses *Tgif2* mRNA expression. The repression of a gene by a lncRNA is also observed with other lncRNAs, such as *Xist* (Brockdorff et al., 1991; Zhao et al., 2008), *Hotair* (Rinn et al., 2007), *Bvht* (Klattenhoff et al., 2013), *Pandar* (Puvvula et al., 2014), *Fendrr* (Grote et al., 2013) and *Airn* (Braidotti et al., 2004; Nagano et al., 2008). We showed that *Gm14230* interacted with Ezh2, which is a subunit of the PRC2 chromatin remodeling complex. Thus, *Gm14230* likely recruits PRC2 to repress *Tgif2* expression. Tgif2 is a homeodomain-containing transcriptional repressor that suppresses *Evi5l* transcription. As shown by the knockdown of *Gm14230* and *Tgif2*, *Gm14230* upregulates *Evi5l* through *Tgif2*. *Gm14230*, *Tgif2* and *Evi5l* are expressed more highly in juvenile than in adult and *Gm14230* titrates the expression of *Tgif2* and *Evi5l*. In the absence of *Gm14230*, *Tgif2* is transcribed in excess, leading to cell cycle arrest and cellular senescence.

The following question remains: how does *Gm14230* maintain cellular juvenescence? *Gm14230* and *Tgif2* are co-regulated by an element in the first intron of *Tgif2*. *Tgif2* suppresses cellular growth and eventually induces cell senescence. *Tgif2* overexpression is observed in ovarian cancer cell lines (Imoto et al., 2000), suggesting that *Tgif2* may function as an oncogene. Similar oncogene-induced senescence has been observed in genes, such as *Ras* (Serrano et al., 1997), *BRAF* (Wajapeyee et al., 2008), *Akt* (Chen et al., 2005) and *E2F* (Denchi et al., 2005). *Gm14230* is believed to titrate the magnitude of *Tgif2* expression. *Gm14230* knockdown also promotes excess *Tgif2* expression, leading to cell senescence. Thus, *Gm14230* represses *Tgif2* expression to maintain cellular juvenescence and prevent premature senescence.

In this study, we identified JAlncs, which are lncRNAs that are selectively highly expressed in juvenile hepatocytes and cardiomyocytes in mice. Among the 62 common JAlncs, *Gm14230* is evolutionarily conserved and is essential for the maintenance of cellular juvenescence. The loss of *Gm14230* leads to cell growth impairment and cell senescence. Therefore, our findings reveal the previously unrecognized role of lncRNAs in the transcriptional network that governs the physiology of juvenile cells.

MATERIALS AND METHODS

Mice

In the previous study (Jam et al., 2018), we performed RNA-seq analysis with the hepatocytes and the cardiomyocytes isolated from the C57BL/6N male mice aged at postnatal day 1 (P1), 7 (P7) and 56 (P56) in triplicate. All animal experiments were approved by the institutional animal care and use committee at Tokyo medical and dental university. All experiments were performed in accordance with the relevant guidelines and regulations. We analyzed the RNA-seq data as below.

RNA-seq and bioinformatics analyses

The lncRNA analysis was performed using our previously reported dataset, which has been deposited to DNA Data Bank of Japan (DDBJ) under the accession number DRA007101 (https://ddbj.nig.ac.jp/DRASearch/submission?acc=DRA007101). The analyses were executed using BioLinux8 (Field et al., 2006). The Fastq files were processed with Fastx trimmer (FASTX-Toolkit, http://hannonlab.cshl.edu/fastx_toolkit/) to remove the first base from all the reads because the first base that was

nearest to the annealing site of the sequence primer showed a frequent sequencing error. From the 3′-terminus, the characters with a quality score lower than 20 were trimmed using the Fastq quality trimmer. The reads were removed if their length was shorter than 30 characters after trimming. Reads with more than 80% of characters harboring a quality score higher than 20 were extracted for further analysis. Additionally, reads were removed using the Fastq quality filter if 10% or more of the characters had a quality score less than 30. The Fastq files were processed as described above and mapped to GRCm38 using Tophat2 (Kim et al., 2013). The GTF file of the lncRNA analysis was generated from the Ensembl GTF files by extracting the genes with a gene or transcript biotype of 'lincRNA', 'bidirectional promoter lncRNA' or 'macro lncRNA'. The differential gene expression was analyzed using Cuffdiff (Trapnell et al., 2010) and the lncRNA GTF file.

To identify the juvenility-associated lncRNAs (JAlncs), we processed the fragments per kilobase of transcript per million fragments sequenced (FPKM) data as follows. First, lncRNAs that showed 0 FPKM for all samples were removed. Next, those lncRNAs that were detected in one sample or less among the P1 triplicates were removed. The lncRNAs with fold changes of greater than 2 at both P1 and P7 compared to those at P56 were included. Some lncRNAs had specific expression in juvenile phases and expression in P56 was not detected at all (FPKM=0). In those cases, a fold change is impossible to calculate. To include the lncRNAs that were expressed in juvenile phases but not at all in the adult phase, those lncRNAs were included if two or three of the three samples for both P1 and P7 showed more than 0 FPKM.

Heatmaps were generated using MeV (http://mev.tm4.org). The expression was visualized with the Integrative Genomics Viewer (http://software.broadinstitute.org/software/igv/). Open reading frame analysis was performed with ORFfinder (https://www.ncbi.nlm.nih.gov/orffinder/). The evolutionary conservation between *Gm14230* and *DLGAP4-AS1-205* was assessed using ClustalW (Thompson et al., 1994). To investigate the regulatory elements associated with gene expression, the ChIP-atlas database was utilized (http://chip-atlas.org). microRNA target sites in *Gm14230* were searched using LncBase Predicted v.2 (http://carolina.imis.athena-innovation.gr/diana_tools/web/index.php) and RegRNA2.0 (http://regrna2.mbc.nctu.edu.tw/). For the quantification of *Gm14230* in microRNA-deficient conditions, we reanalyzed the deposited data of RNA-seq performed in *Dicer*-knockout (KO) mouse embryonic stem (ES) cells (GSE55338), *Dicer*-KO spermatocytes (GSE63166) and *Ago2*-KO ES cells (GSE80454). We downloaded the fastq files from the Sequence Read Archive (SRA) and calculated the expression levels as transcripts per million (TPM) using Salmon (Patro et al., 2017).

Conservation analysis

The interspecies conservation of lncRNA between mouse and human were analyzed as below. Sequences of the mouse common JAlncs were obtained from the Ensembl database. Sequences of the human lncRNAs were obtained from Ensembl BioMart (https://www.ensembl.org/biomart). A database of human lncRNAs were generated using the makeblastdb command of BLAST (version 2.7.1). The sequence similarity between mouse and human lncRNAs was assessed by running blastn, where a mouse JAlnc sequence was queried in the generated human lncRNA database. To quantitatively compare the extent of conservation, E-values and bit scores were used. The interspecies similarity in the secondary structure of lncRNAs were assessed using RNAforester, a tool that compares RNA secondary structures via forest alignment (Höchsmann et al., 2003, 2004, https://bibiserv.cebitec.uni-bielefeld.de/rnaforester). RNAforester calculates similarity between a pair of RNA structures and calculates the relative scores that are upper-bounded by 1, which is the score for equal structures.

Cell culture

The Hepa1-6 cell line was purchased from The European Collection of Authenticated Cell Cultures (ECACC). The NIH3T3 and ONS-76 cell lines were purchased from Japanese Collection of Research Bioresources (JCRB) Cell Bank. NIH3T3 and ONS-76 cells were used in this study because these cell lines exhibited hallmarks of the cellular senescence prominently among tested cell lines. Hepa1-6 and NIH3T3 cell lines were cultured in Dulbecco's modified Eagle's medium (DMEM) containing 10% fetal bovine serum (FBS) and penicillin/streptomycin. ONS-76 cells were cultured in RPMI containing 10% fetal bovine serum (FBS) and penicillin/streptomycin. In the knockdown experiments, Lipofectamine RNAiMAX (Invitrogen) was used to transfect the siRNA duplexes at 10 nM: *Gm14230*-siRNA1 (5′-CGAAGACCACUUGGGAUAAdTdT-3′), *Gm14230*-siRNA2 (5′-GGUGCUAAAGGACCAGUUGdTdT-3′), *Gm14230*-siRNA3 (5′-GCUCAGUCGGCUCAGAGUAdTdT-3′), *AC153370.2* (5′-CUGCUGACGUCUGCCGGCAdTdT-3′), *DLGAP4-AS1-205* (5′-CGGUGCGAUUGGUCCCGUUdTdT-3′), *Evi5l* (Sigma-Aldrich, Mission siRNA SASI_Mm01_00020067) and siRNA negative control (Applied Biosystems, AM4611). The siRNA negative control was designed to have no significant sequence similarity with mouse or human transcript sequences, and used for the purpose of establishing a baseline and eliminating the systemic effects produced by transfection.

pCAGIP-*EGFP* has been previously described (Mori et al., 2009). pcDNA4-TO-HA-*Tgif2* was generated by PCR cloning human *Tgif2*. For the plasmid transfection, Lipofectamine 2000 (Invitrogen) was used according to the manufacturer's instructions. The cell images were obtained using EVOS FL (Thermo Fisher Scientific). The number of cells per field was counted manually.

For the staining of SA-β-Gal activity, 7 days after the transfection, the cells were fixed with 3% (v/v) formaldehyde in PBS, washed with PBS twice, and incubated with the staining solution [5 mM $K_3Fe(CN)_6$, 2 mM $MgCl_2$, 150 mM NaCl, 30 mM citric acid/phosphate buffer, 5 mM $K_4Fe(CN)_6$, and 1 mg/ml X-Gal] for 16 h at 37°C.

For the zeocin-induced cellular senescence model, cells were treated with zeocin (100 µg/ml) for 48 h and were continued to be cultured in fresh medium (Robles and Adami, 1998; Mao et al., 2016).

Gene expression analysis

The total RNA was extracted using TRIzol reagent (Thermo Fisher Scientific). The extracted RNA was quantified using a NanoDrop Lite Spectrophotometer (Thermo Fisher Scientific) and reverse transcribed using a high-capacity RNA-to-cDNA kit (Applied Biosystems) and a PCR thermal cycler (Dice; Takara) according to the manufacturer's instructions. qPCR was performed using a LightCycler 480 SYBR Green I Master Kit on a LightCycler 480 instrument (Roche) using the reverse transcribed cDNA as a template. The specificity and quality of the qPCR amplification was assessed by performing a melting curve analysis. The data were normalized to mouse *Polr2a* or *Tubb5* as indicated in the figure legends. The primers used for the qPCR are listed in Table S3.

RNA editing analysis

The sequence of *Gm14230* in the NIH3T3 cells and mouse neonatal hepatocytes (at P1) was analyzed by cloning the *Gm14230* cDNA. The PCR products were cloned into a T-vector using a Mighty TA-cloning Kit (Takara). The sequences were analyzed for each of the colonies. The RNA editing analysis was performed using cyanoethylation as previously described (Suzuki et al., 2015). Briefly, 4 µl of the RNA sample adjusted to 0.125 µg/µl was mixed with 30 µl of the CE solution (50% ethanol and 1.1 M triethylammonium acetate, pH 8.6) and 4 µl of 15.2 M acrylonitrile and incubated at 70°C for 60 min. The reaction was quenched by the addition of 162 µl of RNase-free water on ice. The RNA was extracted by ethanol precipitation and reverse transcribed as described in the 'Gene expression analysis' section. The sequences of the synthesized cDNAs were analyzed by direct sequencing.

Subcellular fractionation

For the subcellular fractionation of the cultured cells, the cells were trypsinized, pelleted by centrifugation (300 ***g*** for 2 min), resuspended in lysis buffer (50 mM Tris-HCl, pH 8.0, 140 mM NaCl, 1.5 mM $MgCl_2$, and 0.5% NP-40) and incubated at 4°C for 5 min. Then, the lysates were centrifuged at 300 ***g*** for 2 min. The supernatants were collected as the cytoplasmic fractions. To wash the nuclear fraction, chilled PBS was added to the pellet, followed by centrifugation at 300 ***g*** for 2 min. The supernatants were discarded, and the pellet remained as the nuclear fraction. For the RNA extraction, 1 ml of TRIzol reagent (Thermo Fisher Scientific) was added to both fractions. The RNA was extracted as described in the 'Gene expression analysis' section.

RNA-FISH

Fluorescent *in situ* hybridization for *Gm14230* in NIH3T3 cells was performed as described previously (Sone et al., 2007). More specifically, *Gm14230* cDNA was cloned and PCR-amplified using the forward primer: 5′-GAGTGTTTCCGGAGCGCCTAC-3′ and the T7 site-adding reverse primer: 5′-TTAATACGACTCACTATAGG TCACCCAGCATTCAGTC-CGC-3′. A repetitive sequence was searched by RepeatMasker (www.repeatmasker.org/). The PCR product was used as a template for RNA synthesis. Digoxigenin-labeled RNA probes were prepared by using RNA-labeling mixture (Roche) and T7 RNA polymerase (Roche). NIH3T3 cells were fixed with 4% paraformaldehyde for 10 min at room temperature (RT) followed by a PBS wash. Cells were then permeabilized with PBS containing 0.5% Tween 20 for 5 min. After incubation in prehybridization buffer (50% formamide, 1× Denhardt's solution, 2× SSC, 10 mM EDTA, 100 µg/ml yeast tRNA, 0.01% Tween 20) for 2 h at 55°C, cells were incubated with synthesized RNA probes diluted in hybridization buffer (50% formamide, 1× Denhardt's solution, 2× SSC, 10 mM EDTA, 100 µg/ml yeast tRNA, 0.01% Tween 20, 5% dextran sulfate) overnight at 55°C. The hybridized probes were detected with standard immunohistochemical procedures using a mouse monoclonal anti-DIG primary antibody (1:200, 21H8, #ab420, Abcam) and Alexa Fluor 488-conjugated anti-mouse secondary antibody (ThermoFisher Scientific). Images were acquired using Nikon C1si.

SDS-PAGE and western blot analysis

The cells were harvested in RIPA lysis buffer containing 25 mM Tris-HCl (pH 7.6), 150 mM NaCl, 1% NP-40, 1% sodium deoxycholate and 0.1% SDS. The protein samples (10 µg per lane) were separated by SDS-PAGE and transferred to a Hybond-P PVDF membrane (GE Healthcare). Western blotting was performed using the antibodies against the following proteins: (1) P16 ARC (1:1000, Abcam, ab51243), (2) P27 Kip1 (1:1000, Cell Signaling, #3698), (3) γH2Ax (1:1000, Cell Signaling, #9718), (4) Srsf7 (1:1000, Thermo Fisher Scientific, PA5-39482) and (5) β-actin (1:2000, Cell Signaling, #5125). Secondary antibodies conjugated with horseradish peroxidase (Thermo Fisher Scientific, anti-mouse-IgG, 32430 and anti-rabbit-IgG 32460) were used at a 1:1000 dilution. The immunoreactive bands were detected using Chemi-Lumi One L or Chemi-Lumi One Ultra (Nacalai Tesque). Uncropped blots were provided in Fig. S6C.

Immunocytochemistry

NIH3T3 cells transfected with siRNA or a plasmid vector were fixed with 4% paraformaldehyde for 10 min at RT, permeabilized with 0.1% Triton X-100 for 2 min at RT, blocked with 2% FBS, and incubated with antibody against Ki67 (1:400, Cell Signaling, #12202), active caspase 3 (1:200, Abcam, ab2302), cleaved PARP (1:200, Cell Signaling, #9544) and vimentin (1:80, Santa Cruz Biotechnology, sc-6260) at 4°C overnight. After washing PBS, cells were incubated with anti-mouse-IgG conjugated to Alexa Fluor 488 and anti-rabbit-IgG conjugated to Alexa Fluor 546 (1:1000, Invitrogen). Nuclei were stained with DAPI (Invitrogen).

RIP-qPCR

Crosslinking was performed by adding 3.3% formaldehyde to the medium, followed by incubation at RT for 10 min. The reaction was stopped by the addition of 6.5 µM glycine and further incubated for 5 min at RT. After a few washes for several minutes each with cold PBS, the cells were lysed with NETN buffer [20 mM Tris-Cl, pH 8.0, 1 mM EDTA, 100 mM NaCl, and 0.5% (v/v) Nonidet P-40] and collected by scraping. The cell lysates were treated with 10 units of Turbo DNase at 37°C for 10 min. After centrifugation at 20,000 ***g*** for 5 min at 4°C, a part of the supernatant was collected as the input sample. The remaining supernatant was incubated with the anti-Ezh2 antibody (Cell Signaling, 5246S) or control rabbit IgG (Santa Cruz Biotechnology) conjugated to Dynabeads Protein A (10002D, Life Technologies) overnight at 4°C. The Dynabeads complexes were collected using a magnet stand (Dynal, Thermo Fisher Scientific) and washed with 170 µl CLIP wash buffer (1× PBS without Mg^{2+} or Ca^{2+}, 0.1% SDS, and 0.5% NP-40) twice for 10 min and then with 170 µl high-salt wash buffer (5× PBS without Mg^{2+} or Ca^{2+}, 0.1% SDS, and 0.5% NP-40) twice for 10 min. Then, the beads were resuspended with RIPA buffer (25 mM Tris-HCl, pH 7.6, 150 mM NaCl, 1% NP-40, 1% sodium deoxycholate and 0.1% SDS). The crosslinks were reversed by incubating the beads with proteinase K at 70°C for 3 h. The supernatants were collected as the RIP samples, and the RNA was extracted using TRIzol as described in the 'Gene expression analysis' section. The qPCR quantification was performed based on standard curves. The relative enrichment by the Ezh2 antibody was calculated by normalizing to the amounts of RNA pulled down by the control IgG.

Native ChIP assays

Chromatin immunoprecipitation was performed as previously described (Nimura et al., 2009) with NIH3T3 cells transfected with *Gm14230* siRNA_2 or negative control siRNA at 20 nM. Primer sequences are listed in Table S4. The data and the image for the interspecies conservation at the mouse *Tgif2* locus was obtained from the UCSC genome browser (https://genome.ucsc.edu/).

Statistical analysis

The mean±s.d. is presented for all quantified data. The statistical significance between two experimental groups is indicated by an asterisk, and the comparisons were performed using Student's *t*-tests. *P*-values less than 0.05 were considered significant.

Acknowledgements

We would like to thank all the laboratory members from the Molecular Neuroscience Research Center (MNRC) for their helpful discussions and sincere cooperation. This study was also supported by the Central Research Laboratory at Shiga University of Medical Science (SUMS).

Competing interests

The authors declare no competing or financial interests.

Author contributions

Conceptualization: A.T., Y.K., T.M., J.-P.B., M.M.; Methodology: A.T., Y.K., F.A.J., H.Y., M.M.; Software: Y.K.; Validation: A.T., Y.K., T.M., F.A.J., M.M.; Formal analysis: A.T., Y.K., T.M., F.A.J., H.Y., M.M.; Investigation: A.T., Y.K., T.M., F.A.J., H.Y., M.M.; Resources: A.T., Y.K., T.M., M.M.; Data curation: A.T., Y.K., T.M., F.A.J., H.Y., J.-P.B., T.S., Y.M., I.T., M.M.; Writing - original draft: A.T., Y.K., T.M., J.-P.B., M.M.; Writing - review & editing: A.T., Y.K., T.M., F.A.J., H.Y., J.-P.B., T.S., Y.M., I.T., M.M.; Visualization: T.M., F.A.J., H.Y., M.M.; Supervision: J.-P.B., T.S., Y.M., I.T., M.M.; Funding acquisition: Y.M., I.T., M.M.

Funding

M.M. is supported by a research grant from the Kanae Foundation for the Promotion of Medical Science, the Miyata foundation bounty for pediatric cardiovascular research from the Miyata Cardiac Research Promotion Foundation, the Sumitomo Foundation, the Meiji Yasuda Life Foundation of Health and Welfare, the Kato Memorial Bioscience Foundation, the Nagao Memorial Fund, the Japan Epilepsy Research Foundation (JERF) and the Hoansha Foundation. This study was supported by Grants-in-Aid for Scientific Research for Young Scientists from the Japan Intractable Diseases (Nanbyo) Research Foundation. This study was supported by Ministry of Education, Culture, Sports, Science and Technology (MEXT) KAKENHI grant number 15K15387, Japan Society for the Promotion of Science (JSPS) KAKENHI grant numbers 15H01486 and 18K07788, and the Leading Initiative for Excellent Young Researchers (LEADER) grant number 5013323.

Supplementary information

Supplementary information available online at
http://jcs.biologists.org/lookup/doi/10.1242/jcs.227801.supplemental

References

Alcorta, D. A., Xiong, Y., Phelps, D., Hannon, G., Beach, D. and Barrett, J. C. (1996). Involvement of the cyclin-dependent kinase inhibitor p16 (INK4a) in replicative senescence of normal human fibroblasts. *Proc. Natl. Acad. Sci. USA* **93**, 13742-13747.

Alvarez-Dominguez, J. R., Bai, Z., Xu, D., Yuan, B., Lo, K. A., Yoon, M. J., Lim, Y. C., Knoll, M., Slavov, N., Chen, S. et al. (2015). De novo reconstruction of adipose tissue transcriptomes reveals long non-coding RNA regulators of brown adipocyte development. *Cell Metab.* **21**, 764-776.

Anderson, A. E., Taniguchi, K., Hao, Y., Melhuish, T. A., Shah, A., Turner, S. D., Sutherland, A. E. and Wotton, D. (2017). Tgif1 and Tgif2 repress expression of the RabGAP Evi5l. *Mol. Cell. Biol.* **37**, e00527-16.

Batista, P. J. and Chang, H. Y. (2013). Long noncoding RNAs: cellular address codes in development and disease. *Cell* **152**, 1298-1307.
Bertone, P., Stolc, V., Royce, T. E., Rozowsky, J. S., Urban, A. E., Zhu, X., Rinn, J. L., Tongprasit, W., Samanta, M., Weissman, S. et al. (2004). Global identification of human transcribed sequences with genome tiling arrays. *Science* **306**, 2242-2246.
Braidotti, G., Baubec, T., Pauler, F., Seidl, C., Smrzka, O., Stricker, S., Yotova, I. and Barlow, D. P. P. (2004). The Air Noncoding RNA: An Imprinted cis-silencing Transcript. *Cold Spring Harb. Symp. Quant. Biol.* **69**, 55-66.
Brockdorff, N., Ashworth, A., Kay, G. F., Cooper, P., Smith, S., McCabe, V. M., Norris, D. P., Penny, G. D., Patel, D. and Rastan, S. (1991). Conservation of position and exclusive expression of mouse Xist from the inactive X chromosome. *Nature* **351**, 329-331.
Cabili, M. N., Dunagin, M. C., McClanahan, P. D., Biaesch, A., Padovan-Merhar, O., Regev, A., Rinn, J. L. and Raj, A. (2015). Localization and abundance analysis of human lncRNAs at single-cell and single-molecule resolution. *Genome Biol.* **16**, 1-16.
Chen, Z., Trotman, L. C., Shaffer, D., Lin, H.-K., Dotan, Z. A., Niki, M., Koutcher, J. A., Scher, H. I., Ludwig, T., Gerald, W. et al. (2005). Crucial role of p53-dependent cellular senescence in suppression of Pten-deficient tumorigenesis. *Nature* **436**, 725-730.
Collado, M., Medema, R. H., García-Cao, I., Dubuisson, M. L. N., Barradas, M., Glassford, J., Rivas, C., Burgering, B. M. T., Serrano, M. and Lam, E. W.-F. (2000). Inhibition of the phosphoinositide 3-kinase pathway induces a senescence-like arrest mediated by p27 Kip1. *J. Biol. Chem.* **275**, 21960-21968.
Damas, N. D., Marcatti, M., Côme, C., Christensen, L. L., Nielsen, M. M., Baumgartner, R., Gylling, H. M., Maglieri, G., Rundsten, C. F., Seemann, S. E. et al. (2016). SNHG5 promotes colorectal cancer cell survival by counteracting STAU1-mediated mRNA destabilization. *Nat. Commun.* **7**, 13875.
Denchi, E. L., Attwooll, C., Pasini, D. and Helin, K. (2005). Deregulated E2F Activity Induces Hyperplasia and Senescence-Like Features in the Mouse Pituitary Gland. *Mol. Cell. Biol.* **25**, 2660-2672.
Ellis, B. C., Molloy, P. L. and Graham, L. D. (2012). CRNDE: a long non-coding RNA involved in CanceR neurobiology, and development. *Front. Genet.* **3**, 1-15.
Fagagna, F. A., Reaper, P. M., Clay-Farrace, L., Fiegler, H., Carr, P., von Zglinicki, T., Saretzki, G., Carter, N. P. and Jackson, S. P. (2003). A DNA damage checkpoint response in telomere-initiated senescence. *Nature* **426**, 194-198.
Ferrè, F., Colantoni, A. and Helmer-Citterich, M. (2016). Revealing protein-lncRNA interaction. *Brief. Bioinform.* **17**, 106-116.
Field, D., Tiwari, B., Booth, T., Houten, S., Swan, D., Bertrand, N. and Thurston, M. (2006). Open software for biologists: from famine to feast. *Nat. Biotechnol.* **24**, 801-803.
Ge, Y., Yan, X., Jin, Y., Yang, X., Yu, X., Zhou, L., Han, S., Yuan, Q. and Yang, M. (2015). MiRNA-192 and miRNA-204 directly suppress lncRNA HOTTIP and interrupt GLS1-mediated glutaminolysis in hepatocellular carcinoma. *PLoS Genet.* **12**, e1005825.
Gott, J. M. and Emeson, R. B. (2000). Functions and mechanisms of RNA editing. *Annu. Rev. Genet.* **34**, 499-531.
Gregory, R. I., Yan, K.-P., Amuthan, G., Chendrimada, T., Doratotaj, B., Cooch, N. and Shiekhattar, R. (2004). The Microprocessor complex mediates the genesis of microRNAs. *Nature* **432**, 235-240.
Grote, P., Wittler, L., Hendrix, D., Koch, F., Währisch, S., Beisaw, A., Macura, K., Bläss, G., Kellis, M., Werber, M. et al. (2013). The Tissue-Specific lncRNA Fendrr Is an Essential Regulator of Heart and Body Wall Development in the Mouse. *Dev. Cell* **24**, 206-214.
Hangauer, M. J., Vaughn, I. W. and McManus, M. T. (2013). Pervasive transcription of the human genome produces thousands of previously unidentified long intergenic noncoding RNAs. *PLoS Genet.* **9**, e1003569.
Höchsmann, M., Töller, T., Giegerich, R. and Kurtz, S. (2003). Local similarity in RNA secondary structures. *Proc. IEEE Comput. Soc. Bioinforma. Conf.* **2**, 159-168.
Höchsmann, M., Voss, B. and Giegerich, R. (2004). Pure multiple RNA secondary structure alignments: a progressive profile approach. *IEEE/ACM Trans. Comput. Biol. Bioinforma.* **1**, 53-62.
Hon, C.-C., Ramilowski, J. A., Harshbarger, J., Bertin, N., Rackham, O. J. L., Gough, J., Denisenko, E., Schmeier, S., Poulsen, T. M., Severin, J. et al. (2017). An atlas of human long non-coding RNAs with accurate 5′ ends. *Nature* **543**, 199-204.
Imoto, I., Pimkhaokham, A., Watanabe, T., Saito-Ohara, F., Soeda, E. and Inazawa, J. (2000). Amplification and overexpression of TGIF2, a novel homeobox gene of the TALE superclass, in ovarian cancer cell lines. *Biochem. Biophys. Res. Commun.* **276**, 264-270.
Jalali, S., Bhartiya, D., Lalwani, M. K., Sivasubbu, S. and Scaria, V. (2013). Systematic transcriptome wide analysis of lncRNA-miRNA interactions. *PLoS ONE* **8**, e53823.
Jam, F. A., Kadota, Y., Mendsaikhan, A., Tooyama, I. and Mori, M. (2018). Identification of juvenility-associated genes in the mouse hepatocytes and cardiomyocytes. *Sci. Rep.* **8**, 3132.
Ji, P., Diederichs, S., Wang, W., Böing, S., Metzger, R., Schneider, P. M., Tidow, N., Brandt, B., Buerger, H., Bulk, E. et al. (2003). MALAT-1, a novel noncoding RNA, and thymosin β4 predict metastasis and survival in early-stage non-small cell lung cancer. *Oncogene* **22**, 8031-8041.
Kapranov, P., Willingham, A. T. and Gingeras, T. R. (2007a). Genome-wide transcription and the implications for genomic organization. *Nat. Rev. Genet.* **8**, 413-423.
Kapranov, P., Cheng, J., Dike, S., Nix, D. A., Duttagupta, R., Willingham, A. T., Stadler, P. F., Hertel, J., Hackermuller, J., Hofacker, I. L. et al. (2007b). RNA maps reveal new RNA classes and a possible function for pervasive transcription. *Science* **316**, 1484-1488.
Kawahara, Y., Zinshteyn, B., Sethupathy, P., Iizasa, H., Hatzigeorgiou, A. G. and Nishikura, K. (2007). Redirection of silencing targets by adenosine-to-inosine editing of miRNAs. *Science* **315**, 1137-1140.
Khalil, A. M., Guttman, M., Huarte, M., Garber, M., Raj, A., Rivea Morales, D., Thomas, K., Presser, A., Bernstein, B. E., van Oudenaarden, A. et al. (2009). Many human large intergenic noncoding RNAs associate with chromatin-modifying complexes and affect gene expression. *Proc. Natl. Acad. Sci. USA* **106**, 11667-11672.
Kim, D., Pertea, G., Trapnell, C., Pimentel, H., Kelley, R. and Salzberg, S. L. (2013). TopHat2: accurate alignment of transcriptomes in the presence of insertions, deletions and gene fusions. *Genome Biol.* **14**, R36.
Klattenhoff, C. a, Scheuermann, J. C., Surface, L. E., Bradley, R. K., Fields, P. a, Steinhauser, M. L., Ding, H., Butty, V. L., Torrey, L., Haas, S. et al. (2013). Braveheart, a long noncoding RNA required for cardiovascular lineage commitment. *Cell* **152**, 570-583.
Kopp, F. and Mendell, J. T. (2018). Functional classification and experimental dissection of long noncoding RNAs. *Cell* **172**, 393-407.
Lim, S. R. and Hertel, K. J. (2001). Modulation of survival motor neuron pre-mRNA splicing by inhibition of alternative 3′ splice site pairing. *J. Biol. Chem.* **276**, 45476-45483.
Mao, P., Liu, J., Zhang, Z., Zhang, H., Liu, H., Gao, S., Rong, Y. S. and Zhao, Y. (2016). Homologous recombination-dependent repair of telomeric DSBs in proliferating human cells. *Nat. Commun.* **7**, 12154.
Mas-Ponte, D., Carlevaro-Fita, J., Palumbo, E., Hermoso Pulido, T., Guigo, R. and Johnson, R. (2017). LncATLAS database for subcellular localization of long noncoding RNAs. *RNA* **23**, 1080-1087.
Melhuish, T. A., Gallo, C. M. and Wotton, D. (2001). TGIF2 interacts with histone deacetylase 1 and represses transcription. *J. Biol. Chem.* **276**, 32109-32114.
Mercer, T. R., Dinger, M. E. and Mattick, J. S. (2009). Long non-coding RNAs: insights into functions. *Nat. Rev. Genet.* **10**, 155-159.
Modzelewski, A. J., Hilz, S., Crate, E. A., Schweidenback, C. T. H., Fogarty, E. A., Grenier, J. K., Freire, R., Cohen, P. E. and Grimson, A. (2015). Dgcr8 and Dicer are essential for sex chromosome integrity during meiosis in males. *J. Cell Sci.* **128**, 2314-2327.
Mori, M., Nakagami, H., Koibuchi, N., Miura, K., Takami, Y., Koriyama, H., Hayashi, H., Sabe, H., Mochizuki, N., Morishita, R. et al. (2009). Zyxin mediates actin fiber reorganization in epithelial–mesenchymal transition and contributes to endocardial morphogenesis. *Mol. Biol. Cell* **20**, 3115-3124.
Nagano, T., Mitchell, J. A., Sanz, L. A., Pauler, F. M., Ferguson-Smith, A. C., Feil, R. and Fraser, P. (2008). The Air Noncoding RNA Epigenetically Silences Transcription by Targeting G9a to Chromatin. *Science* **322**, 1717-1720.
Nakagawa, S., Ip, J. Y., Shioi, G., Tripathi, V., Zong, X., Hirose, T. and Prasanth, K. V. (2012). Malat1 is not an essential component of nuclear speckles in mice. *RNA* **18**, 1487-1499.
Ngondo, R. P., Cirera-Salinas, D., Yu, J., Wischnewski, H., Bodak, M., Vandormael-Pournin, S., Geiselmann, A., Wettstein, R., Luitz, J., Cohen-Tannoudji, M. et al. (2018). Argonaute 2 is required for extra-embryonic endoderm differentiation of mouse embryonic stem cells. *Stem Cell Rep.* **10**, 461-476.
Nimura, K., Ura, K., Shiratori, H., Ikawa, M., Okabe, M., Schwartz, R. J. and Kaneda, Y. (2009). A histone H3 lysine 36 trimethyltransferase links Nkx2-5 to Wolf-Hirschhorn syndrome. *Nature* **460**, 287-291.
Nishikura, K. (2010). Functions and regulation of RNA editing by ADAR deaminases. *Annu. Rev. Biochem.* **79**, 321-349.
Paralkar, V. R., Taborda, C. C., Huang, P., Yao, Y., Kossenkov, A. V., Prasad, R., Luan, J., Davies, J. O. J., Hughes, J. R., Hardison, R. C. et al. (2016). Unlinking an lncRNA from its associated cis element. *Mol. Cell* **62**, 104-110.
Patro, R., Duggal, G., Love, M. I., Irizarry, R. A. and Kingsford, C. (2017). Salmon provides fast and bias-aware quantification of transcript expression. *Nat. Methods* **14**, 417-419.
Ponting, C. P., Oliver, P. L. and Reik, W. (2009). Evolution and functions of long noncoding RNAs. *Cell* **136**, 629-641.
Puvvula, P. K., Desetty, R. D., Pineau, P., Marchio, A., Moon, A., Dejean, A. and Bischof, O. (2014). Long noncoding RNA PANDA and scaffold-attachment-factor SAFA control senescence entry and exit. *Nat. Commun.* **5**, 5323.
Rinn, J. L. and Chang, H. Y. (2012). Genome regulation by long noncoding RNAs. *Annu. Rev. Biochem.* **81**, 145-166.
Rinn, J. L., Kertesz, M., Wang, J. K., Squazzo, S. L., Xu, X., Brugmann, S. a, Goodnough, L. H., Helms, J. a, Farnham, P. J., Segal, E. et al. (2007).

Functional demarcation of active and silent chromatin domains in human HOX loci by noncoding RNAs. *Cell* **129**, 1311-1323.

Robles, S. J. and Adami, G. R. (1998). Agents that cause DNA double strand breaks lead to p16(INK4a) enrichment and the premature senescence of normal fibroblasts. *Oncogene* **16**, 1113-1123.

Serrano, M., Lin, A. W., McCurrach, M. E., Beach, D. and Lowe, S. W. (1997). Oncogenic ras provokes premature cell senescence associated with accumulation of p53 and p16INK4a. *Cell* **88**, 593-602.

Sigova, A. A., Mullen, A. C., Molinie, B., Gupta, S., Orlando, D. A., Guenther, M. G., Almada, A. E., Lin, C., Sharp, P. A., Giallourakis, C. C. et al. (2013). Divergent transcription of long noncoding RNA/mRNA gene pairs in embryonic stem cells. *Proc. Natl. Acad. Sci. USA* **110**, 2876-2881.

Sommer, B., Köhler, M., Sprengel, R. and Seeburg, P. H. (1991). RNA editing in brain controls a determinant of ion flow in glutamate-gated channels. *Cell* **67**, 11-19.

Sone, M., Hayashi, T., Tarui, H., Agata, K., Takeichi, M. and Nakagawa, S. (2007). The mRNA-like noncoding RNA Gomafu constitutes a novel nuclear domain in a subset of neurons. *J. Cell Sci.* **120**, 2498-2506.

Suzuki, T., Ueda, H., Okada, S. and Sakurai, M. (2015). Transcriptome-wide identification of adenosine-to-inosine editing using the ICE-seq method. *Nat. Protoc.* **10**, 715-732.

Teranishi, T., Tanaka, M., Kimoto, S., Ono, Y., Miyakoshi, K., Kono, T. and Yoshimura, Y. (2004). Rapid replacement of somatic linker histones with the oocyte-specific linker histone H1foo in nuclear transfer. *Dev. Biol.* **266**, 76-86.

Thompson, J. D., Higgins, D. G. and Gibson, T. J. (1994). CLUSTAL W: improving the sensitivity of progressive multiple sequence alignment through sequence weighting, position-specific gap penalties and weight matrix choice. *Nucleic Acids Res.* **22**, 4673-4680.

Trapnell, C., Williams, B. A., Pertea, G., Mortazavi, A., Kwan, G., van Baren, M. J., Salzberg, S. L., Wold, B. J. and Pachter, L. (2010). Transcript assembly and quantification by RNA-Seq reveals unannotated transcripts and isoform switching during cell differentiation. *Nat. Biotechnol.* **28**, 511-515.

van Deutekom, J. C. T. (2001). Antisense-induced exon skipping restores dystrophin expression in DMD patient derived muscle cells. *Hum. Mol. Genet.* **10**, 1547-1554.

Vanderschuren, L., Niesink, R. J. and Van Ree, J. M. (1997). The neurobiology of social play behavior in rats. *Neurosci. Biobehav. Rev.* **21**, 309-326.

Wajapeyee, N., Serra, R. W., Zhu, X., Mahalingam, M. and Green, M. R. (2008). Oncogenic BRAF induces senescence and apoptosis through pathways mediated by the secreted protein IGFBP7. *Cell* **132**, 363-374.

Washietl, S., Kellis, M. and Garber, M. (2014). Evolutionary dynamics and tissue specificity of human long noncoding RNAs in six mammals. *Genome Res.* **24**, 616-628.

Wilusz, J. E., Sunwoo, H. and Spector, D. L. (2009). Long noncoding RNAs: functional surprises from the RNA world. *Genes Dev.* **23**, 1494-1504.

Xu, Z., Wei, W., Gagneur, J., Perocchi, F., Clauder-Münster, S., Camblong, J., Guffanti, E., Stutz, F., Huber, W. and Steinmetz, L. M. (2009). Bidirectional promoters generate pervasive transcription in yeast. *Nature* **457**, 1033-1037.

Zeng, Y. and Cullen, B. R. (2002). RNA interference in human cells is restricted to the cytoplasm. *RNA* **8**, 855-860.

Zerbino, D. R., Achuthan, P., Akanni, W., Amode, M. R., Barrell, D., Bhai, J., Billis, K., Cummins, C., Gall, A., Girón, C. G. et al. (2018). Ensembl 2018. *Nucleic Acids Res.* **46**, D754-D761.

Zhao, J., Ohsumi, T. K., Kung, J. T., Ogawa, Y., Grau, D. J., Sarma, K., Song, J. J., Kingston, R. E., Borowsky, M. and Lee, J. T. (2010). Genome-wide identification of polycomb-associated RNAs by RIP-seq. *Mol. Cell* **40**, 939-953.

Zhao, J., Sun, B. K., Erwin, J. A., Song, J.-J. J. and Lee, J. T. (2008). Polycomb proteins targeted by a short repeat RNA to the mouse X chromosome. *Science* **322**, 750-756.

Zheng, G. X. Y., Do, B. T., Webster, D. E., Khavari, P. A. and Chang, H. Y. (2014). Dicer-microRNA-Myc circuit promotes transcription of hundreds of long noncoding RNAs. *Nat. Struct. Mol. Biol.* **21**, 585-590.

Zheng, Y., Lorenzo, C. and Beal, P. A. (2016). DNA editing in DNA/RNA hybrids by adenosine deaminases that act on RNA. *Nucleic Acids Res.* **45**, 3369-3377.